# Non- Flexural Parallel Piston Movement across CMUT with Substrate-Embedded Springs

Byung Chul Lee[1*], Amin Nikoozadeh[1], Kwan Kyu Park[2], and Butrus(Pierre) T. Khuri-Yakub[1],
[1]Khuri-Yakub Ultrasonics Group, E. L. Ginzton Laboratory, Stanford University, Stanford, CA, USA
[2]School of Mechanical Engineering, Hanyang University, Seoul, Republic of Korea
[*]Corresponding Email : bclee79@stanford.edu

***Abstract*— In this paper, we introduce a modified fabrication method for CMUTs with substrate-embedded springs (post-CMUTs or PCMUTs) to increase the fabrication yield. This modified fabrication process includes three additional steps from the previous process: vacuum cleaning prior to the wafer bonding step, thermal oxidation of the silicon piston top plate, and preservation of the 150-nm buried oxide (BOX) layer on top of the 250 nm Si layer of the bonded SOI wafer. These modifications increased the fabrication yield from 10% to 60%. For these newly fabricated PCMUT devices, we measured the electrical input impedance with a precision impedance analyzer, the plate displacement with a laser Doppler vibrometer (LDV), and the output pressure with a calibrated hydrophone. The measured electrical input impedance matches well with the FEA simulation results; the LDV measurement in air confirmed a non-flexural plate displacement; and the hydrophone measurement showed a peak-to-peak acoustic pressure of 27.6 kPa at a distance of 3.6 mm in immersion, corresponding to 1.05 MPa at the face of the transducer, for a particular test 2-D array element.**

***Keywords—Ultrasound; PCMUT; substrate-embedded springs; Non-flexural parallel piston movement; Average volume displacement***

## I. INTRODUCTION

A CMUT with substrate-embedded springs, called post-CMUT (PCMUT), has been developed that improves the transducer performance over the classical CMUT architecture [1]. As shown in Fig. 1(a), which represents a cross-sectional 2-D PCMUT element, PCMUT has a thick piston top plate supported by several silicon posts. These thick piston top plate and silicon posts provide a non-flexural parallel piston movement converting large electrostatic energy more efficiently to acoustic energy. Besides increasing the average vertical displacement by its parallel piston motion, this PCMUT structure can generate over 90% of its fill factor so that both vertical and lateral improvement can maximize the average volume displacement. Previously, 3-D finite element analysis (FEA) was used not only to successfully demonstrate this non-flexural parallel piston movement across the active moving plate, but also to comprehensively simulate this device performance [2].

In [3], we presented a fabrication process of second-generation PCMUTs to experimentally buttress our 3-D FEA simulation results. The fabrication process provides a flexible platform as implementing variable devices such as 82-element 1-D arrays, a single element device for high-intensity focused ultrasound (HIFU), and 2-D arrays. However, since large area of the thin, brittle 250-nm Si top plate layer was exposed during the following post process steps such as dicing, wire-bonding, and packaging, the process yield resulted in less than 10% [Fig. 1(b)]. As the key role of this thin 250-nm Si top plate is to preserve the vacuum inside the vacuum gap, the damage of this layer causes the device failure. Furthermore, although the non-uniform shape of the piston top plates begets minor effect to the device performance, this irregular shape creates some defects during the fabrication process [Fig. 1(c)].

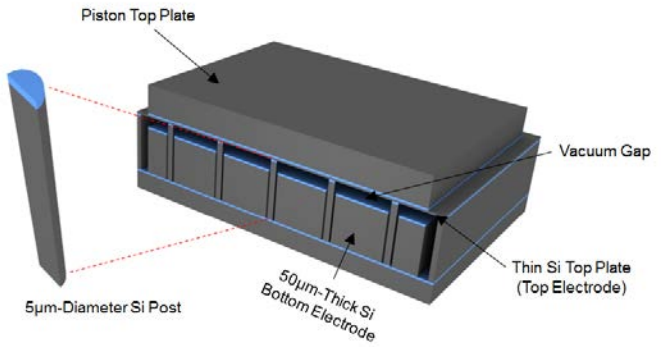


(a)

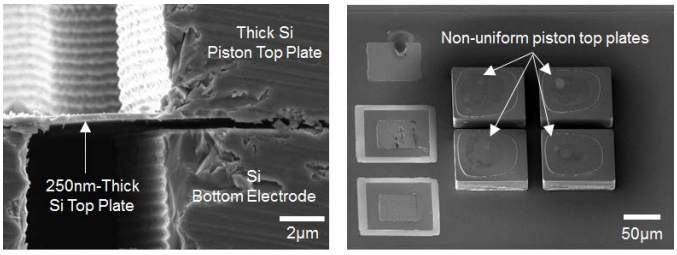


(b) (c)

**Fig. 1.** (a) 3-D perspective view of a cross-sectional 2D PCMUT element. (b) Zoomed-in cross-sectional SEM image of the thin Si top plate. (c) 3-D perspective SEM image of second-generation PCMUT.

In this paper, we introduce a modified PCMUT fabrication method increasing device yield and experimentally prove the non-flexural parallel piston movement of recently fabricated PCMUTs. This modified fabrication process includes three additional steps from the previous process: vacuum cleaning

prior to the wafer bonding step, thermal oxidation of the silicon piston top plate, and preservation of the 150-nm buried oxide (BOX) layer on top of the 250 nm Si layer of the bonded SOI wafer. For these newly fabricated PCMUT devices, we measured PCMUT device specifications of the electrical input impedance, the plate displacement, and the output pressure as a validation of the non-flexural parallel piston motion as well as large average volume displacement.

## II. METHOD

### A. PCMUT Device Structure

The aforementioned downsides of the previous fabrication process in [3] were the exposure of the fragile thin silicon top plate as well as the top surface damage of the piston top plates after the consecutive process steps. As shown in Fig. 2, the left-hand side illustrates one PCMUT cell structure after the previous fabrication process. In order to solve the weaknesses of the previous fabrication step, we tuned this vulnerable PCMUT device structure by adding silicon dioxide protection layers on both the piston top plate and the thin silicon top plate as shown in the right-hand side of Fig. 2. Since silicon dioxide is an amorphous material, it fortifies the brittle thin silicon top plate from fractures in its crystalline direction. Also, silicon dioxide has good etching selectivity so that it has been used as an etch-stop material. By growing the silicon dioxide on top of the piston top plates, it can protect the silicon surface from the following silicon etching process.

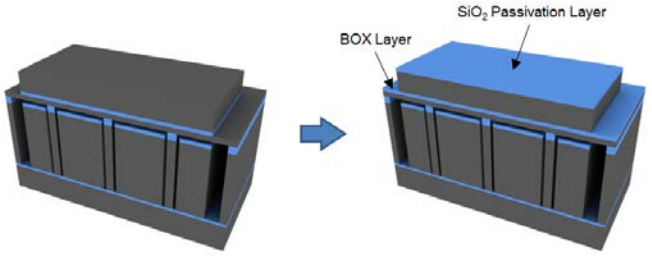


**Fig. 2.** 3-D perspective view of a single PCMUT element with the cross-sectional cut of the fourth quadrant cell.

Figure 3 shows 3-D perspective view of a single 2-D PCMUT element with the cross section of the fourth quadrant cell. Four identical cells compose a single 2-D PCMUT element. From the 3-D FEA simulation study [2], while the four-cell structure sacrifices the fill factor due to the increment of the bonding area, its fractional bandwidth surpasses that of the single-cell single PCMUT element. All the dimensional parameters are labeled in Fig. 3 and listed in Table I. We considered previous fabrication data from [3] that the undercut and footing effect during the post etching reduced the size of the post diameter from 5 μm to 4 μm. The thickness deviation from the wafer polishing was also taken into account in piston top plate 2 thickness, $t_{plate2}$. In the thin top plate 1, $t_{plate1}$, we adjusted the effective thickness from 250 nm to 310 nm by contemplating the Young's modulus of 150 nm BOX layer. From the given dimension of PCMUT, we simulated using a commercial FEA simulator, ANSYS (ANSYS, Inc., Canonsburg, PA). This 2-D PCMUT element resulted in a center frequency of about 2MHz with a -3-dB fractional bandwidth of about 100% in immersion for the medical ultrasound imaging.

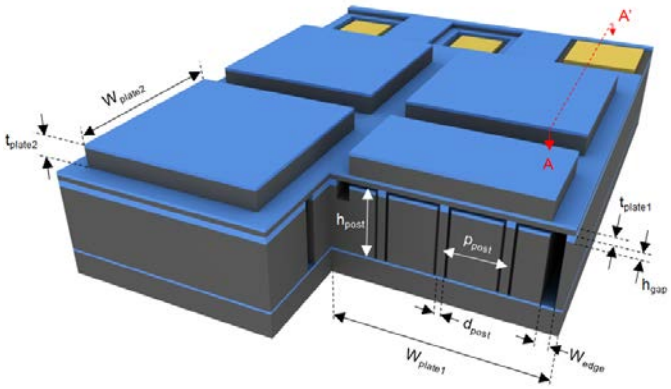


**Fig. 3.** 3-D perspective view of a single 2-D PCMUT element with the cross section of the fourth quadrant cell.

TABLE I. DEVICE PARAMETERS

| **Post Diameter ($d_{post}$)** | **Post Height ($h_{post}$)** | **Post Pitch ($P_{pitch}$)** | **Spring Number ($N_{spring}$)** |
|---|---|---|---|
| 4 μm | 50 μm | 30μm | 3 x 3 |
| **Plate 1 Width ($W_{plate1}$)** | **Plate 1 Thickness ($t_{plate1}$)** | **Plate 1 Material** | **Peripheral Edge ($W_{edge}$)** |
| 140μm | 310nm | $SiO_2$ / Si | 5μm |
| **Plate 2 Width ($W_{plate2}$)** | **Plate 2 Thickness ($t_{plate2}$)** | **Plate 2 Material** | **Effective Gap ($h_{gap}$)** |
| 120μm | 23 μm | $SiO_2$ / Si | 250nm |

### B. Modified Fabrication Process

In order to increase the device yield and make the PCMUT structure robust, three modified process steps are added in the previous fabrication process. First, we inserted vacuum cleaning step prior to the wafer bonding process. This step enhanced the wafer bonding quality, since it completely eliminated all the contaminants from the deep trenches as well as the chamber of the wafer bonder. Second, 150 nm thin silicon dioxide layer was thermally grown on top of the piston top plate. This gave an excellent protection layer during etching the thin silicon top plate. In addition, this high temperature oxidation can anneal silicon damages caused by the wafer grinding and polishing. Lastly, instead of the blank etch of a BOX layer from the previous fabrication process, we preserved 150 nm buried oxide (BOX) layer on top of the 250 nm Si layer and patterned it for the front side electrode opening. This also provided a good physical and electrical passivation of the PCMUT devices.

As starting with a SOI substrate wafer having a device layer of 50 μm, it is oxidized and patterned to determine the device width of the PCMUT [Fig. 4(a)]. After proceeding the second oxidation for defining the effective gap height [Fig.

4(b)], shallow trenches of silicon and silicon dioxide are etched into the device layer using a reactive ion etching (RIE) process in order to electrically connect all the four cells to a bottom electrode [Fig. 4(c)]. Next, patterning of silicon posts and bottom electrode isolation are performed using a deep reactive ion etching (DRIE) process [Fig. 4(d)]. A chemical hydrophilization treatment is conducted on both the patterned wafer and another SOI wafer. The patterned wafer is loaded in the vacuum bonder under the vacuum condition of $5.0 \times 10^{-5}$ mbar for 20 mins. After this vacuum cleaning process, the other chemical treated wafer is bonded on top of the patterned wafer [Fig 4(e)]. As represented in Fig. 4(e) as a dash lie, the handle layer of the top SOI wafer is then polished to the thickness of the PCMUT piston top plate. 100 nm-thick thermal oxide is grown by the oxidation furnace [Fig. 4(f)]. This high temperature oxidation and annealing step provides the protection layer of piston top plates. The oxide and piston top plate are patterned using DRIE [Fig. 4(g)]. After exposing the BOX layer of the top SOI wafer, the BOX layer is opened generating the front-side electrical connection to the thin silicon top plate as a top electrode and the bottom silicon device layer as a bottom electrode [Fig. 4(h)]. We electrically separate each device by patterning the thin silicon top plate [Fig. 4(i)]. Another oxide is etched to expose the bottom electrode [Fig. 4(j)]. Finally, aluminum is deposited on the whole wafer and patterned to determine the electrical pads [Fig. 4(k)].

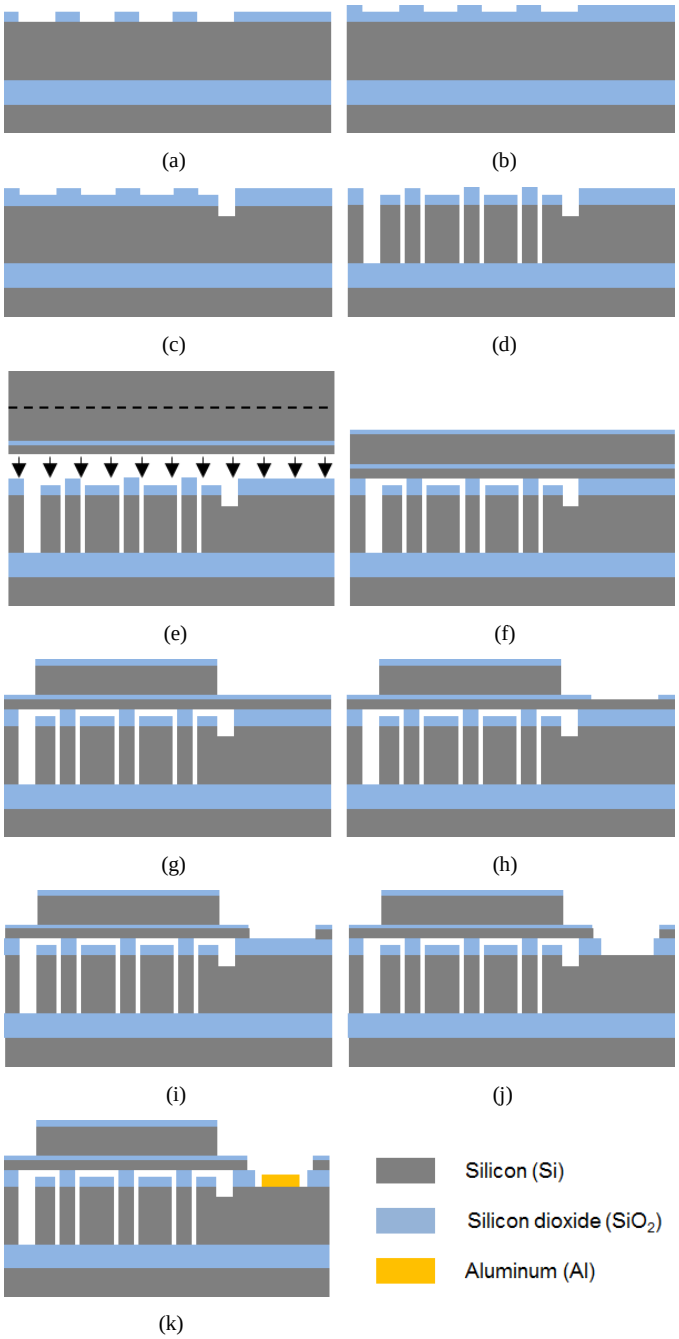


**Fig. 4.** Fabrication Process Flow. The cross-sectional view of A-A' line in Fig. 3. is shown, i.e. the first quadrant PCMUT cell with a bottom electrode pad.

### *C. Experimental Device Characterization*

SEM images were taken from a FEI Helios NanoLab 600i DualBeam FIB/SEM. Focused ion beam (FIB) sectioned the PCMUT to clearly visualize the cross section of the fabricated PCMUT. A impedance analyzer (4294A, Agilent Technologies, Inc.) was used to record the electrical imput impedance in air. Dynamic plate displacement was measured with a laser Doppler vibrometer (OFV-511, Polytec GmbH). The area scan of the displacement across the moving plate was conducted with precision XY stage (U500, Aerotech, Pittsburgh, PA). The XY scanning interval was 20 μm in both direction. Output pressure in oil was measured using a hydrophone (HGL-0200, ONDA Corp.) with its pre-amplifier system. It is attached to a digitizing oscilloscope (Infiniium 54825A, Agilent, Santa Clara, CA) recording the data.

## III. Results and Discussion

Figure 5(a) shows the optical photograph of a fabricated 4-inch wafer, which clearly proves that the modified fabrication process leads to increase the device yield. By inspecting the optical deflection of the thin silicon top plate under an optical microscope and counting the functional PCMUT elements, a process yield of 60 % is achieved. Figure 5(b) shows the SEM image of two different types of 2-D PCMUT elements, a plain piston top plate and a truss-patterned piston top plate. The left-hand side of the SEM image explicitly displays that the silicon dioxide protection layer eliminates the non-uniform etching of

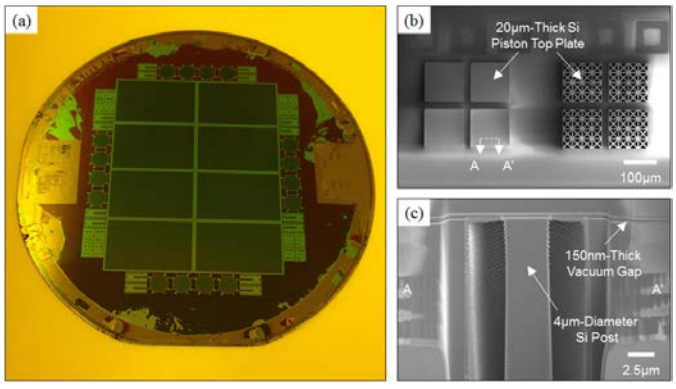


**Fig. 5.** (a) Optical photograph of a whole processed 4-inch wafer. (b) SEM image of two different types of 2D PCMUT elements. (c) Cross-sectional SEM image of A-A' line in Fig. 5(b).

the piston top plate. In addition, this modification allows a truss-patterned piston top plate maintaining the stiffness of the structure itself but reducing the mass. As patterning the piston top plate as a truss shape without changing any other structures and dimensions, the operating frequency and the fractional bandwidth can be precisely modulated. A cross-sectional SEM image of a silicon post is exhibited in Fig. 5(c). Since the piston top plate is obviously propped on this silicon post, 150 nm uniform parallel vacuum gap is observed across the entire piston top plate.

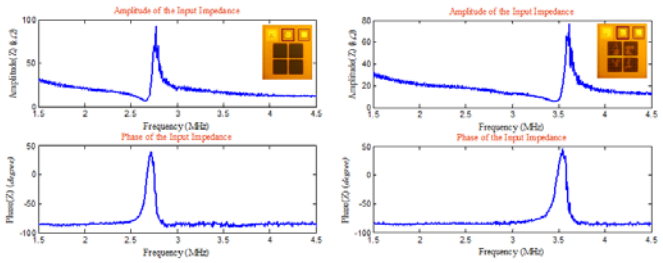


(a) (b)

**Fig. 6.** Electrical input impedance measurement of PCMUTs with (a) a plain and (b) a truss piston top plates.

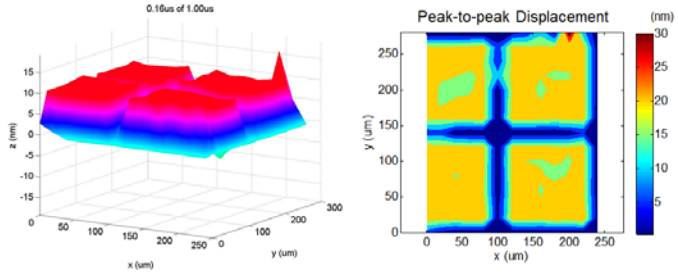


(a) (b)

**Fig. 7.** Dynamic plate displacement measurement of a plain PCMUT: (a) a 3-D perspective view at the moment of the positive maximum peak and (b) a contour plot of a peak-to-peak displacement.

Electrical input impedance of a plain and a truss piston top plates is shown in Fig. 6. While a DC bias voltage of 50 V near 80 % of the collapse voltage was applied, a small AC excitation of 50 mV is superimposed with sweeping the frequencies. The large amplitude and phase changes of each impedance infer high electromechanical coupling factor due to the large parallel displacement. The transformation of the plain piston top plate through the truss pattern only alters the operating frequency with constant amplitude and phase [Fig.6(b)]. With a DC bias voltage of 35 V superposed an unipolar rectangular pulse of 10V and 200 ns duration, Fig. 7 explicitly demonstrates the non-flexural parallel piston movement of the plain PCMUT. A peak in Fig. 7(a) is an edge reflection error from the LDV. Figure 8 shows the measured acoustic pressure of a truss PCMUT in oil after normalizing the hydrophone sensitivity. A single sinusoidal pulse of 70 Vpp amplitude and 588 ns pulse width, superposed on a DC bias voltage of 35V, was applied. A peak-to-peak acoustic pressure of 27.6 kPa at a distance of 3.6 mm, corresponding to 1.05 MPa at the face of the transducer with correction of diffraction and attenuation losses, was measured. From its frequency spectrum, a -3 dB fractional bandwidth of 86% around the center frequency of 1.75 MHz was calculated.

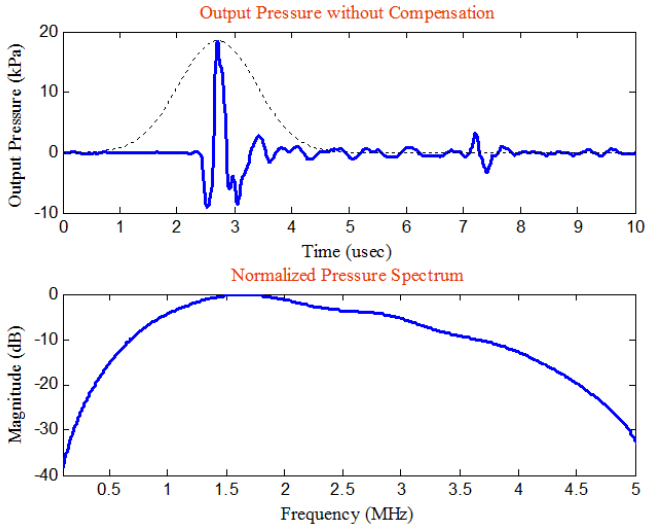


**Fig. 8.** Measured acoustic pressure of a truss PCMUT at 3.6 mm distance. (a) Transient pressure and (b) its frequency spectrum.

## IV. Conclusions

We have modified the previous PCMUT fabrication process, which successfully results in better process yield. From the fabricated PCMUT, all the measurement results such as electrical input impedance, plate displacement, and output pressure assure the non-flexural parallel piston movement of the 2-D PCMUT element. Additionally, from its great fabrication processing versatility, more design flexibility for the operating frequency and -3-dB fractional bandwidth of PCMUT can be achieved. Furthermore, the possible high output pressure generated by the large average volume displacement of a PCMUT will open unprecedented opportunities for medical therapeutic applications as well as diagnostic imaging.

## Acknowledgment

This work was supported by the National Institutes of Health (NIH) and Analog Devices. We fabricated the PCMUT devices at the Stanford Nanofabrication Facility (Stanford, CA), a member of National Nanotechnology Infrastructure Network. We would like to thank Timothy Brand for help with the polishing process. All the SEM pictures were performed at the Stanford Nano Center (SNC) / Stanford Nano-characterization Laboratory (SNL) part of the Stanford Nano Shared Facilities.

## References

[1] A. Nikoozadeh and B. T. Khuri-Yakub, "CMUT with substrate-embedded springs for non-flexural plate movement," in *Proc. IEEE Ultrason. Symp., San Diego, USA*, pp. 1510–1513, Oct. 2010.

[2] B. C. Lee, A. Nikoozadeh, K. K. Park, and B. T. Khuri-Yakub, "Understanding CMUTs with substrate-embedded springs," in *Proc. IEEE Ultrason. Symp., Orlando, USA*, pp. 1008-1011, Oct. 2011.

[3] B. C. Lee, A. Nikoozadeh, K. K. Park, and B. T. Khuri-Yakub, "Fabrication of CMUTs with substrate-embedded springs," in *Proc. IEEE Ultrason. Symp., Prague, Czech Republic* , pp. 1733-1736, Jul. 2013.